Materials Innovations

HΣXA Publishers

Solar Materials | Research Article | http://doi.org/10.54738/MI.2021.1105

Role of Sn Inclusions on Structural, Electrical and Optical Properties of Sb_2S_3

Raies Abdullah[1], Waqar Adil Syed[2], Ahsan Ali[1], Awais Ghani[1], Wasif-ur-Rehman[3], Wajid Ali[4], Muhammad Idrees[5], Naveed Hussain[6]*, Shehzad Ahmed[1]*

1 State Key Laboratory for Mechanical Behavior of Materials, Xi'an Jiaotong University, Xi'an, 710049, China
2 Department of Physics, International Islamic University, Islamabad, 44000, Pakistan
3 MOE Key Laboratory of Thermo-Fluid Science and Engineering, Xi'an Jiaotong University, Xi'an 710049, China
4 Xi'an Key Laboratory of Sustainable Energy Materials Chemistry, School of Chemistry, Xi'an Jiaotong University, Xi'an 710049, China
5 Institute of Micro scale Optoelectronics, Shenzhen University, 518060, Shenzhen, PR China
6 Institute of Fundamental and Frontier Sciences (IFFS), University of Electronic Science and Technology of China, 610054, Chengdu, China

Received: 16 September 2021
Accepted: 17 November 2021
Published: 30 November 2021

Citation: Abdullah R, Syed WA, Ali A, Ghani A, WR, Ali W, Idrees M, Hussain N, Ahmed S (**2021**) Role of Sn Inclusions on Structural, Electrical and Optical Properties of Sb_2S_3. *Materials Innovations 1* (1), 13-20.

***Correspondences**: (Naveed Hussain) n.hussain7766@gmail.com (Shehzad Ahmed) shehzad.stu@gmail.com

Published By Hexa Publishers

Tin antimony sulfide (TAS) thin films are deposited on a glass substrate using a two-source thermal evaporation method. The doping was done to investigate its results on the structural, electrical, and optical properties of tin-antimony sulfide thin films. XRD studies disclosed that annealed films exist in the $Sn_2Sb_2S_5$ phase. The accurate information about the composition and concentration depth of the as-deposited and annealed $Sn_2Sb_2S_5$ thin-films was recorded by the Rutherford backscattering spectroscopy (RBS) technique. The photoconductivity response of these films was also excellent and enhanced with the increasing concentration of tin sulfide. The obtained bandgap was in the range of 1.68-2.31 eV. The thickness of the films was observed to be 240 nm to 336 nm, and the thin films possessed P-type conductivity. Electrical properties are significantly enhanced for the ternary compound $Sn_2Sb_2S_5$ as compared to Sb_2S_3. Results show that antimony tin sulfide has excellent potential in photovoltaic applications.

Keywords: Two sources thermal evaporation, Bandgap, Ternary compound, p-type, Thin film

INTRODUCTION

The demand for sustainable energy using solar cells has risen from a year ago. Since the production of first-generation research and development for enhancement of cell efficiency, new paths towards cost-effective approaches have opened.[1–6] Continuous improvements in photovoltaic devices have made solar energy economically useful. Silicon solar cells have attracted significant attention in recent years and have reached their theoretical limits, but their cost remains high. Current photovoltaics research focuses on earth-abundant materials, dye-sensitized solar cells, non-toxic materials, and nanostructured materials.[7–11] In thin-film photovoltaics, CdTe, GaAs, CuInGaSe, and InP are the leading materials for solar cells. But these materials have high toxicity and involve rare elements, which makes them expensive and harmful to the environment.[12,13] Sulfides based composites are non-toxic, although

associated efficiencies of these photovoltaics are up to 10.1%. As a result of their non-toxicity and abundance, sulfide materials are preferred as absorber layers in solar cells.[14–18] Thin films of pure and doped with Sb_2S_3 are commonly used for photovoltaic devices. The reason for using Sb_2S_3 thin films for energy conversion in solar cells is their properties, such as having a direct bandgap of 1.78–2 eV and a high absorption coefficient of 10^4–$10^5 cm^{-1}$. Solar cells must be manufactured with less expensive materials to be cost effective and easily commercializable, should have a direct bandgap, and high absorption of light.[19] To obtain the required physical properties, the improved method was introduced as the substitution of an atom with fewer or more electrons in its valence shell compared to the host atom. Sb_2S_3 is a member of the V-VI layered semiconductor family. In the family of available chalcogenides, Sb_2S_3 soft films are used in many essential applications, such as highly reactive cooling systems, solar power conversion, solid-state devices, and TV type screens.[20] SnS is also a well-practiced chalcogenide material that has a high optical absorption coefficient, p-type conductivity, and a minimal direct band gap of 1.3-1.4 eV. The energy conversion efficiency of tin sulfide is expected to be up to 32%, which is comparable to crystalline silicon. Whereas SnS is stable in both acid and alkali conditions, All these factors indicate that the substitution of tin sulfide to form SbSnS semiconductors will significantly affect photovoltaic applications.[21,22] In previous literature, many procedures have been used for Sb_2S_3 and SnS deposition, such as chemical bath deposition, chemical vapor deposition, electric deposition, electron beam, spray pyrolysis. In the present studies, Sn-doped using S as a precursor in Sb_2S_3 deposited onto a glass substrate using two source methods, characterized by XRD and SEM for structural and morphological properties, and Rutherford back scattering (RBS) for elemental and compositional analysis. The optical parameters like refractive index (n), extinction coefficient (k), absorption coefficient (α), and optical conductivity was calculated by ellipsometry. Tin generates acceptors level that helps to enhance optical processing. Formation $Sb_2Sn_2S_5$ with different compositional wait percentages of Sn significantly improved the optical structural and electrical properties. Results evidenced that $Sb_2Sn_2S_5$ could bring a potential enhancement in the efficiency of solar cells.

EXPERIMENTAL SETUP

The two-source thermal evaporator was used for doping by the sublimation technique. All elements, i.e., S and Sb, have 4N purity, were used to prepare the initial ingot of Sb_2S_3. Because sulfur can explode when heated rapidly, so as a precaution, we increased the temperature at a relatively slow (15 °C/h) rate. A complete uniformity in composition is accomplished by keeping the mixture at 350 °C for 24 hours. X-rays of powder analysis was performed to study the crystal structure of fabricated materials. X-rays charachterization results showed that only the homogeneous Sb_2S_3 phase was formed in the ingot. Henceforth, the grinded smooth powder form of this ingot is used as the starting material for thermal evaporation.[23,24] SnS and Sb_2S_3 powders were co-evaporated and deposited using a two-source method on a glass substrate, as shown in Figure 1, using sulfur as a precursor in SnS. The quantity of the SnS was divided as 0.1%–0.4% molecular weight compared with the Sb_2S_3 compound source. These materials were vaporized from Al_2O_3 crucibles in the vacuum chamber for sublimation on glass substrates. The pressure of the vacuum-chamber was kept at about 2 x 10^{-4}mbar. After deposition of thin films, we annealed all samples at 425 °C for 24 hours in vacuum-packed glass vessels containing argon gas.

RESULTS AND DISCUSSION

The discussion is mainly focused on physical properties, i.e., structural, optical, and electrical. X-ray diffraction (XRD), scanning electron microscopy (SEM), Rutherford backscattering (RBS), ellipsometry, and Hall measurement techniques were used to obtain experimental data on these important physical properties. The results are discussed in detail to get a comprehensive analysis of the properties of the target material as thin-film. The structure of prepared specimens has been analyzed using x-ray diffraction (XRD) with a Cu K$\alpha\lambda = 1.54\ A$ radiation source. The diffraction spectra of all samples and calculated parameters are indexed in Figure 2(a–c). The orthorhombic phase of $Sn_2Sb_2S_5$ was well-coordinated with (44-0829, JCPDS-ICDD), whereas Sb_2S_3 matched with pdf # 42-1393. Furthermore, it conforms to space group pnma (62) with cell parameters a = 19.59, b = 3.93, and c=11.426. Peaks at 29.2°, 30.6°, 32.1°, 40.6°, 41.7°, 43.9°, 45.0°, and 51.5° have correspondence with planes (114), (312), (042), (143), (108), (047), and (215) which are attributed to $Sb_2Sn_2S_5$.

The sharp peaks in Figure 2(a) support the polycrystalline behavior of these films. The preferential orientation of crystal planes in these thin films is (114). Qualitatively, XRD patterns show that the compositions of $Sn_2Sb_2S_5$ thin films are almost the same as those of the initial material. The diffraction angle 2θ slightly shifted towards higher intensity with the addition of tin sulfide in the Sb_2S_3 because of the addition of Sn atoms in lattice sites to reorient Sb_2S_3 planes. The deviation of dislocation density and associated strain with increasing tin sulfide indicates that values are exponentially dropped, while the minimum is recorded for the film with 0.4% Sn. The lower amount of dislocation density and strain obtained at the high-

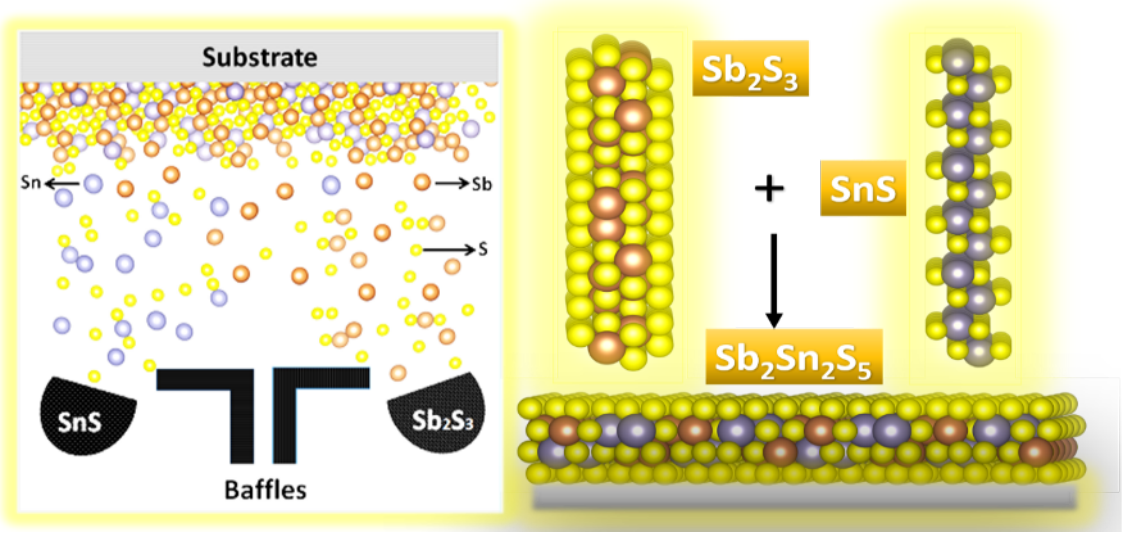

Figure 1. Representation of experimental route using two-Source sublimation technique and formation of the thin film of $Sb_2Sn_2S_5$ using Sb_2S_3 and SnS as starting materials.

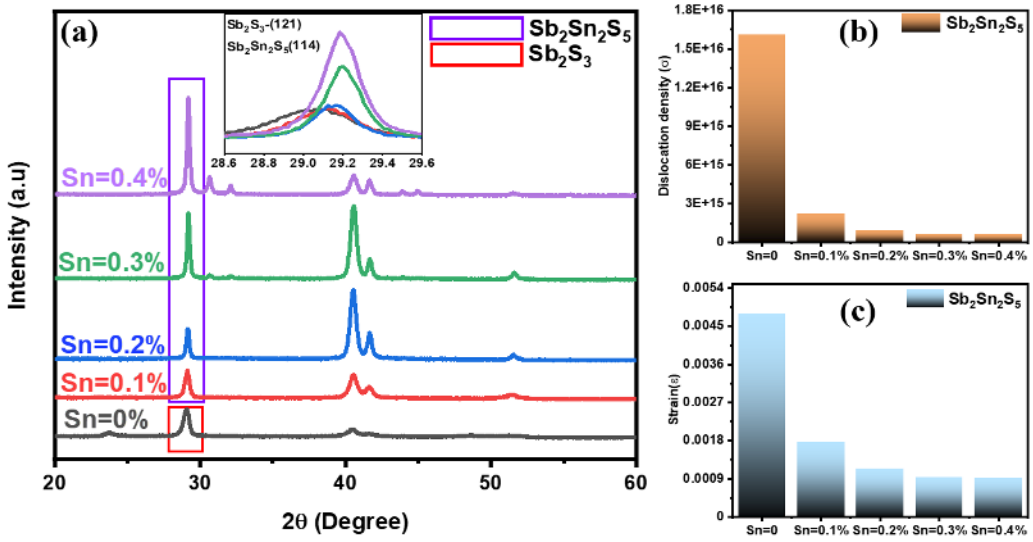

Figure 2. (a) XRD pattern for Tin antimony sulfide thin films with varying concentration of Sn, (b-c) Dislocation and induced lattice strain without substitution of Sn as 0% and after incorporation of Sn from 0.1 to 0.4 %

est Sn concentration reveals the good crystalline effect of tin-antimony sulfide films. While the increase in tin ratio significantly increases the grain size from 21 nm to 41 nm. Small crystallites can fuse to make larger crystallites, resulting in micro-cracks and surface roughness. Annealing is well-known for reducing the stress on film as well as decreasing the d-spacing. XRD patterns indicate that the increase in tin sulfide leads to the improvement of the film's growth in the favored orientation. For surface morphology and compositional analyses, scanning electron microscopy (SEM) and energy-dispersive X-ray spectroscopy (EDS) are used.[25–28] The SEM images of the samples are shown in Figure 3.

The surface of the samples looks smooth and free from roughness, but at the micro-level, the surface samples show little blisters on the surface. Grain size and grain boundary enhancement with an increase in the concentration of SnS small grains merged, and also larger grains split into smaller grains and reoriented themselves, which had an effect on the whole structure. SEM

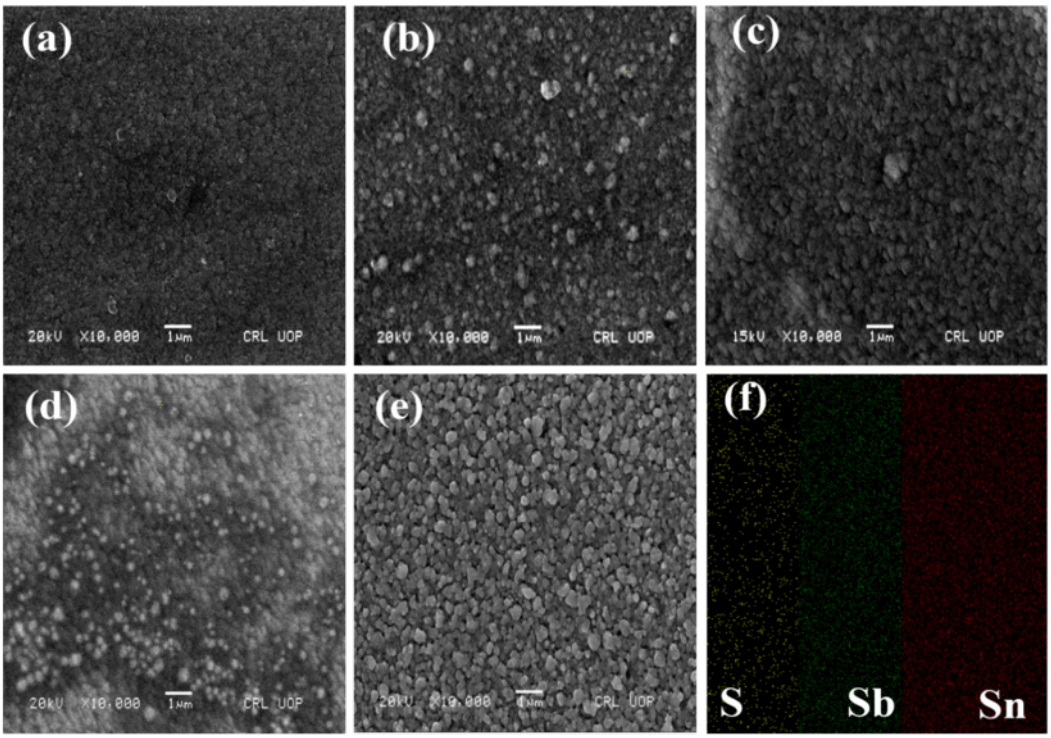

Figure 3. SEM images (a) Thin-film surface of Sb_2S_3 without Sn (b-e) surface of $Sb_2Sn_2S_5$ with Sn (0.1 to 0.4%) (f) EDS mapping of Sn, Sb, and S.

images also indicate a decrease in the roughness of the layer by increasing the concentration of SnS. According to SEM images, we calculated that the average grain size is almost 84.34 nm with beam energy of 20 keV. The creation of a large number of tightly bound particles of different sizes can be seen in these images. The grain size is observed to increase with Sn concentration, as shown in Figure 3. The increase in grain size is due to Sn concentration with improved crystallinity, as calculated from the XRD results. The RBS measurement was carried out on the 5 MV tandem accelerator (5UDH-2, NEC) using a 2.023 MeV He^+ collimated beam.

RBS is a well-described, non-destructive, analytical, quantitative, and unique fundamental investigational accelerator dependent tool. For material examination, it is a distinctive technique broadly used in thin films for thickness, depth profiling of essential elements, and elemental composition. The analyzed depth for incident protons and He^+ions is typically near 20 m and 2 m, respectively.[21,24] The structural analysis of the films was performed using a D-8 Discover diffractometer with Cu Kα radiation (wavelength, $\lambda = 1.54\ A$). The RBS experiments were done on $Sn_2Sb_2S_5$ thin films of varying compositions deposited on glass substrates. The gathered RBS spectra were then fitted by the code RUMP to locate the relative concentrations of a mixture of elements in the films.[29,30] Figure 4 shows the RBS spectra of annealed films of $Sn_2Sb_2S_5$, which proves that the film thickness and concentration of SnS shift the peaks in the higher region. RBS measured a film thickness ranging from 238 nm to 290 nm, which was compared to the thickness measured by ellipsometry, as shown in Figure 4(b). The peaks of the heavy elements (Sn, Sb, and S) can noticeably be separated by the He^+ beam and accordingly can be used to resolve the relative thickness and stoichiometry of the films. The edge arising at a channel just below 1200 is due to the thickness of films present on the substrate.[31]

The energy channel correspondence for tin is 1585; antimony is 1594; while for sulfur, it is 1052. A noticeable change in elemental ratio concerning stoichiometry within the layers has been observed. It was noticed that an edge occurs at 1200. The edge arises due to the excessive enrichment of Sn in the $Sn_2Sb_2S_5$ and corresponds to the unbound Sn content which subsists on the surface. According to the RUMP simulation software, thin-film of Sn 0.4% exhibits the most homogeneous Sn concentration as a function of depth as compared to other studied samples. The thickness of the films estimated by the RBS technique and spectroscopic ellipsometry are in good agreement. Moreover, the deposited films were

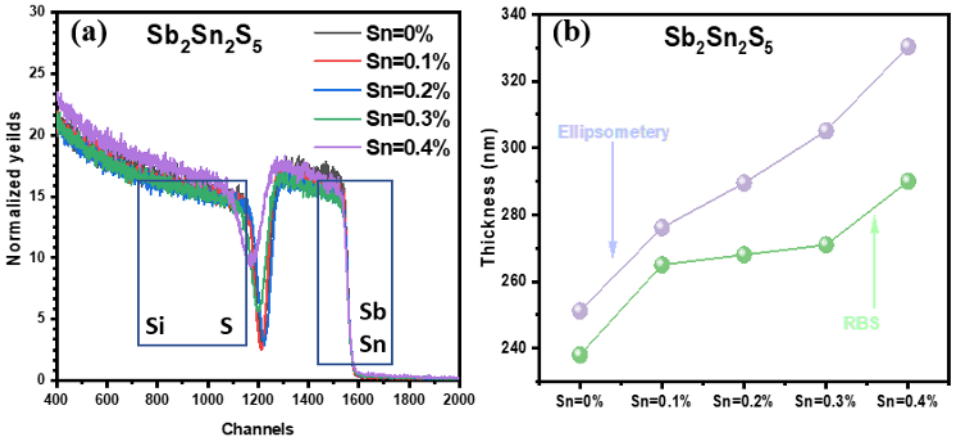

Figure 4. (a) Rutherford backscatteringspectra(RBS) of all S1 samples, (b) Film thickness over increased concentration of Sn by RBS, and its comparison with ellipsometry.

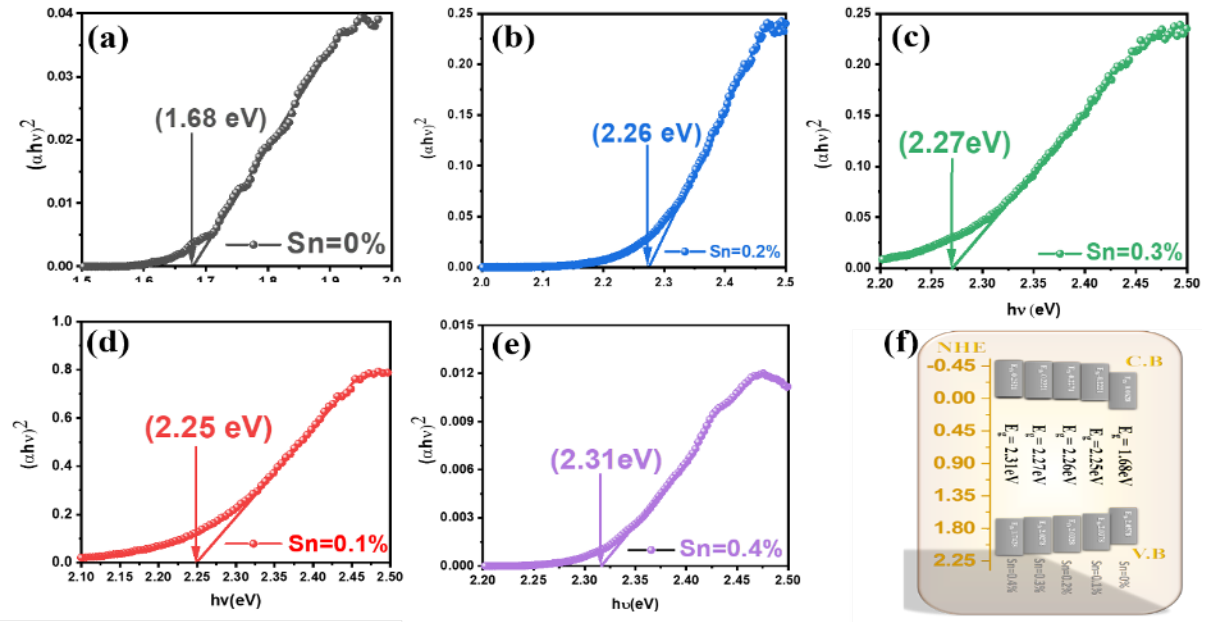

Figure 5. (a-d) Diffuse reflectance spectroscopy (DRS) (a-e) optical band gap estimation of Sb_2S_3 and $Sb_2Sn_2S_5$ using tauc-plot, (d) schematic diagram of band-edge with corresponding NHE potentials.

homogeneous, even, and well adherent to the substrate. The bandgap of the samples was calculated by DRS, which is shown in Figure 5. The calculation was done by using a kabulka maunk and tauc plot method using reflection data.[32,33] The obtained bandgap of a sample with Sn=0%, which represents Sb_2S_3, is 1.68 eV, whereas the formation of $Sb_2Sn_2S_5$ significantly changes the bandgap from 1.68 to 2.31eV, as shown in Figure 5(a-e). The band edges of all samples are shown in Figure 5(f), where conduction and valance band edges widen as tin ratios increase. Substantial favorable placement of the Fermi level near the valance band, i.e., 0.91eV, indicates that it has P-type behavior. The bandgap of samples lies within a visible region, which makes it favorable as an absorber layer of solar cells. Further optical parameters like refractive index, extinction coefficient, and dielectric coefficients were calculated by the ellipsometry technique using an apparatus model named (J.A. Woolam M-200VI) given in Figure 6.

The thickness of the $Sn_2Sb_2S_5$ films is measured by ellipsometry as given above, which is in the range of 251 nm to 330 nm. Optical properties were analyzed from 300 nm to 900 nm in wavelength at room temperature.

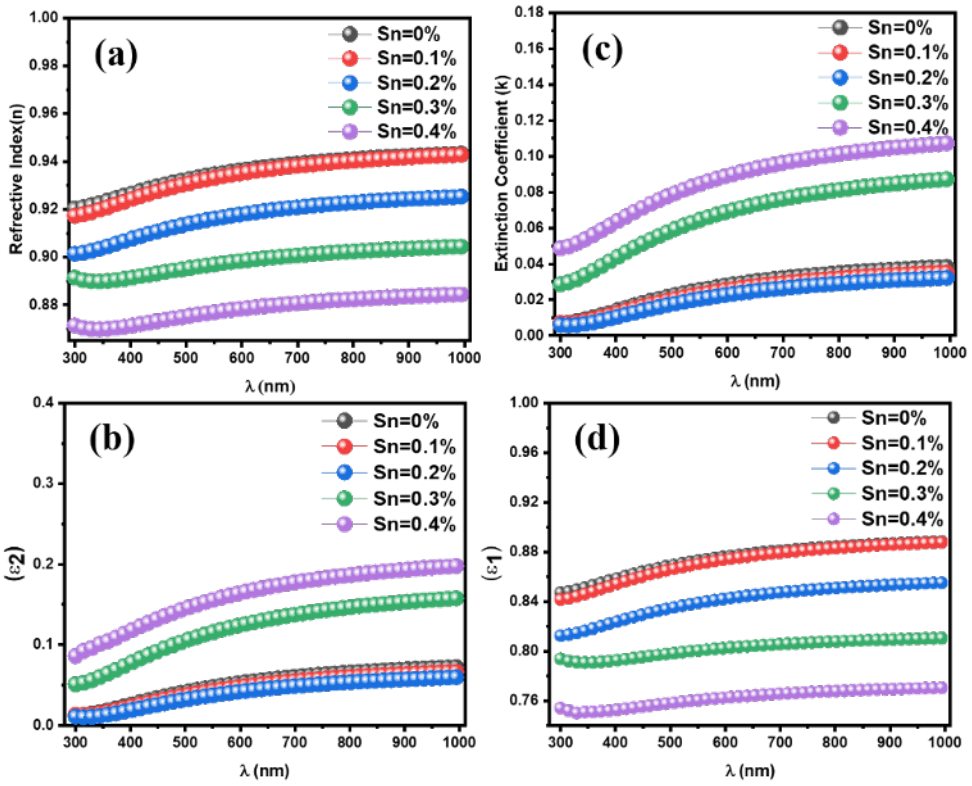

Figure 6. Ellipsometry of $Sb_2Sn_2S_5$ thin films (a) Refractive index (n) (b) Extinction coefficient (k) (c-d) Dielectric constant ε1 and ε2.

The measurements were carried out on prepared thin films with varying tin sulfide concentrations. In Figure 6(a-b), the refractive index (n) and the extinction coefficient "K" were plotted against the wavelength of refraction tells us the penetration of light in the material and the amount that is reflected from the surface. In this context, the refractive index of $Sb_2Sn_2S_3$ has a dominant decrease after substitution of Sn and follows up with an increase ratio. At the same time, a marginal increase was observed in the extinction coefficient for increasing Sn concentration, which indicates the enhanced absorption of light in thin films. The higher value recorded was for Sn=0.4% concentration. Dielectric constants are shown in Figure 6(c-d). They are divided into real (ε_1) and imaginary (ε_2) parts. It decides the response of the material under electromagnetic radiation where real and imaginary are inverse to each other. ε_2 increased with a thickness which directly relates to enhanced absorption of light, but ε_1 describes the retardation of light in the film.[10–12]

The electrical analysis was done by hall measurement using a two-probe method, and by finding the Current-Voltage (IV) response for all samples and results are shown in table 1 and Figure 7. According to the IV curve, we perceive that the examples are highly conductive. By hall measurement, we confirmed that the samples are conductive, having low resistive values, high carrier concentration, and high sheet carrier mobility. The consequences of tin density on thin-film resistivity, mobility, and carrier concentration were measured. Some of the essential parameters are that the area of thin films was 1 cm^2 along with 0.55-tesla constant magnetic field, and one mA current was applied. Calculations show that resistivity lowers its components with increasing tin concentration.[34,35] The resistivity decreases mainly due to an increase in the crystallinity of the material. That enhances free charge carriers, as confirmed by XRD and SEM results. The relation between mobility and resistivity shows that the mobility of carriers and concentration is enhanced. The carrier concentration increases with the tin component until it attains a maximum.

Where Rs stands for sheet resistance; Rho stands for resistivity; Con stands for conductivity; Ns stands for sheet carrier concentration; and μs stands for sheet carrier. Mobility The mobility value without tin is 11.9 $cm^2 V^{-1} s^{-1}$, while Sn=0.4% is 20.4 $cm^2 V^{-1} s^{-1}$. This increase in mobility is attributed to the availability of free electron charge carriers coming from the tin ions. In Sb_2S_3 sites, tin ions are placed and decrease the potential

Table 1. Hall Measurements of the $Sb2Sn_2S_5$ thin films.

Sample	Sheet resistance (ohm/sq)	Resistivity (ohm.cm)	Conductivity (1/ohm-cm)	Sheet carrier concentration($1/cm^2$)	Sheet carrier mobility (cm^2/Vs)
Sn=0.0%	3.21×10^{-1}	1.12×10^{-5}	8.94×10^{4}	-1.37×10^{19}	1.19×10^{1}
Sn=0.1%	1.86×10^{-1}	6.45×10^{-6}	1.55×10^{5}	-1.38×10^{19}	2.44×10^{0}
Sn=0.2%	1.03×10^{-1}	3.64×10^{-6}	2.75×10^{5}	-5.48×10^{18}	1.10×10^{1}
Sn=0.3%	9.93×10^{-2}	2.34×10^{-6}	4.27×10^{5}	-2.16×10^{19}	3.94×10^{0}
Sn=0.4%	1.68×10^{-1}	5.63×10^{-6}	1.78×10^{5}	-1.81×10^{19}	2.04×10^{1}

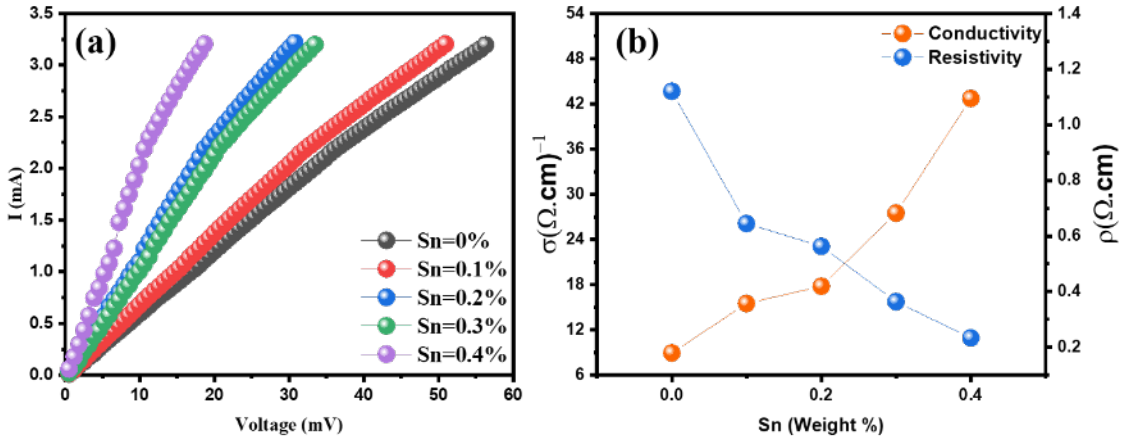

Figure 7. (a) I-V measurements of all samples with different concentrations of Sn, (b) conductivity versus resistivity with a different weight percentage of Sn.

grain barrier. The increase in mobility has a lower value for samples 2 and 3 as compared to other samples, due to the increasing rate of scattering for charge carriers along with the formation of secondary levels, as confirmed by the X-ray diffraction technique. In I-V measurement, the evaluated electrical parameters support that TAS thin films prepared by the two-source method demonstrate better electrical conductivity due to better crystalline quality.

CONCLUSIONS

Tin antimony sulfide was deposited on the glass surface by a two-source evaporation vacuum thermal technique and then annealed in an argon (Ar) gas environment at 350 °C. The crystallite size is calculated by x-ray diffraction and increases with Sn concentration. However, the average particle derived from SEM images is 76.15 nm. We see the homogenous structure of thin films by SEM images and grains are uniformly distributed on thin films. The physical formation of tin-antimony sulfide on thin films is crystalline in nature, with an orthorhombic phase. The material has a direct bandgap that covers the visible region and shows P-type conductivity. The refractive index, extinction coefficient, and dielectric constants prove beneficial in enhancing photon-surface interaction. The electrical properties of $Sb_2Sn_2S_5$ improved after the substitution of Sn with an increase in ratio. These observations suggest that thin-films of Sb_2S_3, in combination with SnS, offer results which open up various possibilities for future work on this theme of the multilayer of the solar cell.

References

1) Ali, N.; Jabeen, M.; Khesro, A.; Ahmed, R.; Alrobei, H.; Kalam, A.; Al-Sehemi, A. G. Combinatorial synthesis of tin antimony sulfide thin films for solar cell application. *International Journal of Energy Research* **2021**, *45* (15), 21527–21533, DOI: 10.1002/er.7180, available at https://doi.org/10.1002/er.7180.
2) Nwofe, P. A.; Sugiyama, M. Microstructural, Optical, and Electrical Properties of Chemically Deposited Tin Antimony Sulfide Thin Films for Use in Optoelectronic Devices. *Physica Status Solidi* **2020**, *217* (9), 1900881, DOI: 10.1002/pssa.201900881, available at https://doi.org/10.1002/pssa.201900881.
3) Ali, N.; Hussain, A.; Ahmed, R.; Shamsuri, W. N. W.; Salam, N. M.; Khenata, R. Fabrication and characterization of 150 nm tin antimony sulfide thin films, a promising window layer material for homojunction solar cells. *Applied Physics A* **2017**, *123* (4), 282, DOI: 10.1007/s00339-017-0879-4, available at https://doi.org/10.1007/s00339-017-0879-4.
4) Devasia, S.; Shaji, S.; Avellaneda, D. A.; Martinez, J. A. A.; Krishnan, B. Tin antimony sulfide (Sn6Sb10S21) thin films by heating chemically deposited Sb2S3/SnS layers: Studies on the structure and their optoelectronic properties. *Journal of Alloys and Compounds* **2020**, *827*, 154256, DOI: 10.1016/j.jallcom.2020.154256, available at https://doi.org/10.1016/j.jallcom.2020.154256.

5) Ali, N.; Ahmed, R.; Shaari, A.; Rahim, I.; Shah, M.; Hussain, A.; Ahmad, N.; Abbas, S. M. Annealing Effects on the Structural and Optical Properties of Thermally Deposited Tin Antimony Sulfide Thin Films. *Brazilian Journal of Physics* **2014**, *44* (6), 733–738, DOI: 10.1007/s13538-014-0255-1.
6) Syed, W. A. A.; Ali, A.; Rafiq, N.; Shah, W. H.; Shah, N. A.; Yasir, M. BaCl2 an efficient replacement of CdCl2 treatment step for thermally deposited CdTe thin film. *Materials Research Express* **2019**, *6* (8), 086438, DOI: 10.1088/2053-1591/ab214f, available at https://doi.org/10.1088/2053-1591/ab214f.
7) Ali, N.; Hussain, A.; Hussain, S. T.; Iqbal, M. A.; Shah, M.; Rahim, I.; Ahmad, N.; Ali, Z.; Hutching, K.; Lane, D.; Syed, W. A. A. Physical Properties of the Absorber Layer Sn2Sb2S5 thin Films for Photovoltaics. *Current Nanoscience* **2013**, *9* (1), 149–152, DOI: 10.2174/157341313805117794, available at https://doi.org/10.2174/157341313805117794.
8) Schock, H. W. Thin film photovoltaics. *Applied Surface Science* **1996**, *92*, 606–616, DOI: 10.1016/0169-4332(95)00303-7.
9) Dhere, N. G. Present status and future prospects of CIGSS thin film solar cells. *Solar Energy Materials and Solar Cells* **2006**, *90* (15), 2181–2190, DOI: 10.1016/j.solmat.2006.02.018.
10) Fthenakis, V. Sustainability of photovoltaics: The case for thin-film solar cells. Sustainability of photovoltaics: The case for thin-film solar cells. 2009; pp 2746–2750.
11) Ali, N.; Hussain, S. T.; Khan, Y.; Ahmad, N.; Iqbal, M. A.; Abbas, S. M. Effect of air annealing on the band gap and optical properties of SnSb2S4 thin films for solar cell application. *Materials Letters* **2013**, *100*, 148–151, DOI: 10.1016/j.matlet.2013.02.097.
12) Fthenakis, V. Sustainability metrics for extending thin-film photovoltaics to terawatt levels. *MRS Bulletin* **2012**, *37* (4), 425–430, DOI: 10.1557/mrs.2012.50, available at https://doi.org/10.1557/mrs.2012.50.
13) Green, M. A. Consolidation of thin-film photovoltaic technology: the coming decade of opportunity. *Progress in Photovoltaics: Research and Applications* **2006**, *14*, 383–392, DOI: 10.1002/pip.702, available at https://doi.org/10.1002/pip.702.
14) Aousgi, F.; Kanzari, M. *Study of the Optical Properties of Sn-doped Sb2S3 Thin Films. Energy Procedings* **2011**, *10*, 313–332, DOI: 10.1016/j.egypro.2011.10.197.
15) Avellaneda, D.; Nair, M. T. S.; Nair, P. K. Photovoltaic structures using chemically deposited tin sulfide thin films. *Thin Solid Films* **2009**, *517* (7), 2500–2502, DOI: https://doi.org/10.1016/j.tsf.2008.11.043, available at https://doi.org/10.1016/j.tsf.2008.11.043.
16) Vinayakumar, V.; Hernández, C. R. O.; Shaji, S.; Avellaneda, D. A.; Martinez, J. A. A.; Krishnan, B. Effects of rapid thermal processing on chemically deposited antimony sulfide thin films. *Materials Science in Semiconductor Processing* **2018**, *80*, 9–17, DOI: 10.1016/j.mssp.2018.02.011, available at https://doi.org/10.1016/j.mssp.2018.02.011.
17) Hussain, N.; Liang, T. X.; Zhang, Q. Y.; Anwar, T.; Huang, Y.; Lang, J. L.; Huang, K.; Wu, H. Ultrathin Bi Nanosheets with Superior Photoluminescence. *Small* **2017**, *13* (36), 1701349, DOI: 10.1002/smll.201701349.
18) Khan, M. A.; Ahmed, A.; Ali, N.; Iqbal, T.; Khan, A. A.; Ullah, M.; Shafique, M. Improved Optical Properties of Tin Antimony Sulphide Thin Films for Photovoltaics. *American Journal of Materials Science and Engineering* **2016**, *4* (1), 1–6, DOI: 10.12691/ajmse-4-1-1.
19) Arslan, M.; Muhammad, R.; Mahmood, A.; Rasheed, R. Effect of thermal annealing on the physical properties of Zn1−x Cu x Se thin films deposited by close spaced sublimation technique. *Acta Metallurgica Sinica (English Letters)* **2013**, *26* (6), 699–706, DOI: 10.1007/s40195-013-0242-5, available at https://doi.org/10.1007/s40195-013-0242-5.
20) Westland, J. C. An Introduction to Structural Equation Models. Structural Equation Models. 2015; pp 1–8, DOI: 10.1007/978-3-319-16507-3_1, available at https://doi.org/10.1007/978-3-319-16507-3_1.
21) Scheu, C.; Kaplan, W. D. Introduction to Scanning Electron Microscopy. 2012; pp 1–37.
22) Toussaint, U. V.; Krieger, K.; Fischer, R.; Dose, V. Depth Profile Reconstruction from Rutherford Backscattering Data. 1999; pp 107–114.
23) Hussain, N.; Rafique, M.; Anwar, T.; Murtaza, M.; Liu, J. C.; Nosheen, F.; Huang, K.; Huang, Y.; Lang, J. L.; Wu, H. A high-pressure mechanism for realizing sub-10 nm tellurium nanoflakes on arbitrary substrates. *2D Materials* **2019**, *6* (4), DOI: 10.1088/2053-1583/ab2540, available at https://doi.org/10.1088/2053-1583/ab2540.
24) Hussain, N.; Zhang, M. H.; Zhang, Q. Y.; Zhou, Z.; Xu, X. Y.; Murtaza, M.; Zhang, R. Y.; Wei, H. H.; Ou, G.; Wang, D.; Wang, K.; Li, J. F.; Wu, H. Large Piezoelectric Strain in Sub-10 Nanometer Two-Dimensional Polyvinylidene Fluoride Nanoflakes. *ACS Nano* **2019**, *13* (4), 4496–4506, DOI: 10.1021/acsnano.9b00104, available at https://doi.org/10.1021/acsnano.9b00104.
25) Hussain, N.; Zhang, Q. Y.; Lang, J. L.; Zhang, R. Y.; Muhammad, M.; Huang, K.; De Villenoisy, T. C.; Ya, H.; Karim, A.; Wu, H. Ultrahigh Room-Temperature Photoluminescence from Few to Single Quintuple Layer Bi2Te3 Nanosheets. *Advance Optical Materials* **2018**, (13), 6–6, DOI: 10.1002/adom.201701322, available at https://doi.org/10.1002/adom.201701322.
26) Ali, A.; Syed, W. A.; Arif, W.; Ahmed, S.; Ghufran, M. A. Environment friendly nanoparticles of quaternary compound Cu0.5MgxSnS4 for possible photovoltaic and photo-catalytic applications. *Materials Research Express* **2019**, *6* (9), 950–955, DOI: 10.1088/2053-1591/ab0f7e, available at https://doi.org/10.1088/2053-1591/ab0f7e.
27) Ali, A.; Liang, Y. P.; Ahmed, S.; Yang, B.; Guo, B. L.; Yang, Y. D. Mutual contaminants relational realization and photocatalytic treatment using Cu2MgSnS4 decorated BaTiO3. *Applied Materials* **2020**, *18*, 100534, DOI: 10.1016/j.apmt.2019.100534, available at https://doi.org/10.1016/j.apmt.2019.100534.
28) Li, L.; Lei, J.; Wu, L.; Pan, F.; Aliofkhazraei, M.; Ali, N.; Chipara, M.; Laidani, N. B. Spectroscopic ellipsometry. Handbook of Modern Coating Technologies. 2021; pp 45–83.
29) Goh, E. S. M.; Chen, T. P.; Sun, C. Q.; Liu, Y. C. Thickness effect on the band gap and optical properties of germanium thin films. *Journal of Applied Physics* **2010**, *107* (2), 24305–24305, DOI: 10.1063/1.3291103, available at https://doi.org/10.1063/1.3291103.
30) Neal, W. E. J. Ellipsometry and its application in the monitoring of surface cleanliness. *Surface Technology* **1984**, *23* (1), 1–28, DOI: 10.1016/0376-4583(84)90072-4, available at https://doi.org/10.1016/0376-4583(84)90072-4.
31) Hussain, N.; Yao, Y. S.; Sagar, R. U. R.; Anwar, T.; Murtaza, M.; Huang, K.; Shehzad, K.; Wu, H.; Wang, Z. M. Quantum-confined blue photoemission in strain-engineered few-atomic-layer 2D germanium. *Nano Energy* **2021**, 83–83, DOI: 10.1016/j.nanoen.2021.105790, available at https://doi.org/10.1016/j.nanoen.2021.105790.
32) Nyamekye, C. K. A.; Bobbitt, J. M.; Zhu, Q. C.; Smith, E. A. The evolution of total internal reflection Raman spectroscopy for the chemical characterization of thin films and interfaces. *Analytical and Bioanalytical Chemistry 2020* (24), 6009–6022, DOI: 10.1007/s00216-020-02510-1, available at https://doi.org/10.1007/s00216-020-02510-1.
33) Knoll, W. Polymer Thin-Films and Interfaces Characterized with Evanescent Light. *Makromol Chem* **1991**, *192* (12), 2827–2856, DOI: 10.1002/macp.1991.021921201.
34) Auciello, O.; Krauss, A. R. Why in-Situ, Real-Time Characterization of Thin-Film Growth-Processes? *MRS Bulletin* **1995**, *20* (5), 14–15, DOI: 10.1557/S0883769400044833.
35) Watts, K. E.; Blackburn, T. J.; Pemberton, J. E. Optical Spectroscopy of Surfaces, Interfaces, and Thin Films: A Status Report. *Analytical Chemistry* **2019**, *91* (7), 4235–4265, DOI: 10.1021/acs.analchem.9b00735.